

# A new way to describe the transition characteristics of a rotating-disk boundary-layer flow

Shintaro Imayama, P. Henrik Alfredsson, and R. J. Lingwood

Citation: [Physics of Fluids](#) **24**, 031701 (2012); doi: 10.1063/1.3696020

View online: <https://doi.org/10.1063/1.3696020>

View Table of Contents: <http://aip.scitation.org/toc/phf/24/3>

Published by the [American Institute of Physics](#)

---

## Articles you may be interested in

[Coupled numerical and theoretical study of the flow transition between a rotating and a stationary disk](#)  
*Physics of Fluids* **16**, 688 (2004); 10.1063/1.1644144

[Laminar-turbulent boundary-layer transition over a rough rotating disk](#)  
*Physics of Fluids* **15**, 2441 (2003); 10.1063/1.1586916

[Experimental characterization of transition region in rotating-disk boundary layer](#)  
*Physics of Fluids* **25**, 034102 (2013); 10.1063/1.4798435

[Boundary layer development in the flow field between a rotating and a stationary disk](#)  
*Physics of Fluids* **24**, 033601 (2012); 10.1063/1.3698406

[The instability of the boundary layer over a disk rotating in an enforced axial flow](#)  
*Physics of Fluids* **23**, 114108 (2011); 10.1063/1.3662133

[The effect of anisotropic and isotropic roughness on the convective stability of the rotating disk boundary layer](#)  
*Physics of Fluids* **27**, 014107 (2015); 10.1063/1.4906091

---

PHYSICS TODAY

WHITEPAPERS

### ADVANCED LIGHT CURE ADHESIVES

Take a closer look at what these environmentally friendly adhesive systems can do

READ NOW

PRESENTED BY  
 MASTERBOND<sup>®</sup>  
ADHESIVES | SEALANTS | COATINGS

## A new way to describe the transition characteristics of a rotating-disk boundary-layer flow

Shintaro Imayama,<sup>1,a)</sup> P. Henrik Alfredsson,<sup>1,b)</sup> and R. J. Lingwood<sup>1,2,c)</sup>

<sup>1</sup>*Linné FLOW Centre, KTH Mechanics, SE-100 44 Stockholm, Sweden*

<sup>2</sup>*University of Cambridge, Cambridge CB23 8AQ, United Kingdom*

(Received 17 January 2012; accepted 28 February 2012; published online 14 March 2012)

A new method of graphically representing the transition stages of a rotating-disk flow is presented. The probability density function contour map of the fluctuating azimuthal disturbance velocity is used to show the characteristics of the boundary-layer flow over the rotating disk as a function of Reynolds numbers. Compared with the variation of the disturbance amplitude (rms) or spectral distribution, this map more clearly shows the changing flow characteristics through the laminar, transitional, and turbulent regions. This method may also be useful to characterize the different stages in the transition process not only for the rotating-disk flow but also for other flows.  
© 2012 American Institute of Physics. [<http://dx.doi.org/10.1063/1.3696020>]

Experimental studies of the flow over a rotating disk show that the boundary-layer is susceptible to an instability that presents itself through the formation of stationary (in the rotating frame) vortices (see Refs. 1–4). This primary instability can be predicted from linear theory; it is of cross-flow type, inviscid in nature and is a convective instability, and may also have a non-zero frequency, i.e., it can be traveling with respect to the disk. However, unless particular traveling modes are deliberately excited, it is the stationary mode that is observed in experiments because it is excited by unavoidable roughnesses on the disk surface. There is also another convectively unstable mode (a viscous mode due to Coriolis and streamline curvature effects), however, for this mode the stationary disturbances have smaller linear growth rates.

Lingwood<sup>5,6</sup> suggested that the onset of transition to turbulence of the rotating-disk boundary-layer is not due directly to the convective instability, but to an absolute instability which occurs above  $R = 507$ . Here the Reynolds number is  $R = r^*(\Omega^*/\nu^*)^{1/2}$ , where  $r^*$  is the radius of the disk at the measurement position,  $\Omega^*$  is the rotational speed of the disk,  $\nu^*$  is the kinematic viscosity of the fluid, and  $*$  denotes a dimensional quantity. By introducing impulsive excitation to the rotating-disk boundary-layer flow, she confirmed experimentally the existence of the absolute instability (above about  $R = 507$ ) by tracking the trajectory of the excited wavepacket (Lingwood<sup>3</sup>). The transition process once triggered probably takes place through a secondary instability.<sup>2,7</sup>

It is the purpose of the present paper to introduce a probability density function (PDF) map of the azimuthal velocity fluctuations to elucidate the changing flow characteristics through the stable and unstable laminar-flow regions, through the transitional region into the fully turbulent region for the rotating-disk flow.

The experimental set-up is a modified version of the one used by Lingwood<sup>5</sup> (see Fig. 1). On the original aluminium-alloy disk a new disk made of glass with a thickness of 24 mm and a diameter of 474 mm has been mounted. The aluminium-alloy disk is connected to a dc-servo motor via a vertical shaft and a pressurized air bearing ensures that the vibrations of the disk are small. The surface of the glass disk is polished resulting in a surface roughness of less than 1  $\mu\text{m}$ ; the rotational imbalance

<sup>a)</sup>Electronic mail: [shintaro@mech.kth.se](mailto:shintaro@mech.kth.se).

<sup>b)</sup>Electronic mail: [phal@mech.kth.se](mailto:phal@mech.kth.se).

<sup>c)</sup>Electronic mail: [lingwood@mech.kth.se](mailto:lingwood@mech.kth.se).

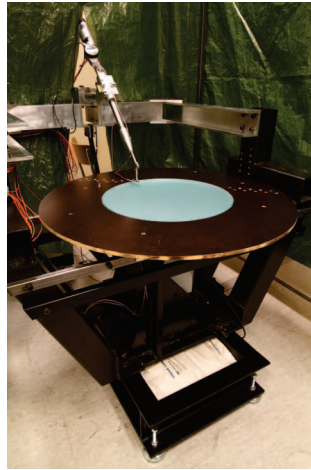


FIG. 1. The experimental set-up of the rotating disk.

is less than  $10\ \mu\text{m}$  at the edge of the glass disk. At the edge of the disk, a fixed wooden annular plate is positioned flush with the disk surface.

A hot-wire probe with a single sensor made of platinum, with a diameter of  $5\ \mu\text{m}$  and  $1\ \text{mm}$  in length, is operated by a constant-temperature anemometer (CTA) with an overheat ratio of 0.8. The sensing element of the hot-wire is oriented in the radial direction, making it mainly sensitive to the azimuthal velocity. The signal from the CTA is digitized using a 16-bit A/D converter at a sampling rate of 720 data points per disk revolution during a 60 s sampling time. The hot-wire probe is mounted on a two-axis, remotely controlled traverse mechanism at  $45^\circ$  to the vertical to limit disturbance of the incoming downward axial flow. The calibration of the hot wire is carried out on the rotating disk using the laminar profile and a modified King's law (for better accuracy at low velocities<sup>8</sup>) is fitted to the calibration data.

The Reynolds number was varied using two methods: (1) varying the rotational disk speed and keeping the probe at a fixed radial position; and (2) varying the radial position of the probe at a fixed rotational disk speed. The experimental conditions are shown in Table I.

The measured azimuthal mean velocity ( $V^*$ ) is plotted in Fig. 2. This corresponds to the azimuthal component of the von Kármán similarity solution for an infinite disk rotating in otherwise quiescent fluid, i.e., a Rossby number of  $Ro = -1$ , as defined, for example, by Lingwood *et al.*<sup>9</sup> The measurements are performed at a fixed radius, and in this case the Reynolds number was changed by varying the rotational speed of the disk. The abscissa is the non-dimensional azimuthal velocity,  $V = V^*/(r^*\Omega^*)$  and the vertical axis is the non-dimensional height from the wall ( $z = z^*(\Omega^*/\nu^*)^{1/2}$ ).

TABLE I. Experimental conditions, where  $r^*$  and  $z$  represent the radial and axial positions of the probe, respectively.

Case	$R$	$r^*$ [mm]	$\Omega^*$ [rpm]	$z$
P01	430	198	690	0.4–16
P02	470	198	822	0.4–16
P03	490	198	890	0.4–16
P03	510	198	963	0.4–16
P04	530	198	1040	0.4–16
P05	550	198	1122	0.4–16
P06	570	198	1205	0.4–16
P07	590	198	1295	0.4–26
P08	610	198	1385	0.4–26
P09	630	198	1480	0.4–26
I01	360–700	116–226	1400	1.3

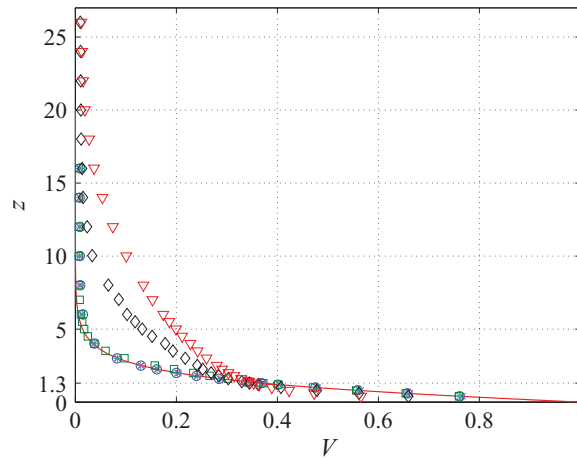


FIG. 2. Mean azimuthal velocity profiles at  $R = 430$  ( $\circ$ ),  $470$  ( $*$ ),  $510$  ( $\times$ ),  $550$  ( $\square$ ),  $590$  ( $\diamond$ ),  $630$  ( $\nabla$ ). Solid line is the laminar theory profile.

For Reynolds numbers in the range  $R = 430$ – $510$ , the measured profiles correspond well to the theoretical laminar profile shown as a solid line, except far away from the disk where the smallness of the azimuthal velocity makes the hot-wire measurements inaccurate. Between  $R = 510$  and  $R = 550$  the nonlinear influence of the growing disturbances causes the mean azimuthal velocity to deviate from the theoretical laminar profile. With further increases in Reynolds number, this effect grows. At  $R = 630$ , the velocity profile has completely changed from the basic laminar one, giving a larger velocity gradient close to the wall and a dramatically increased boundary-layer thickness; both characteristics of the development of a turbulent boundary-layer.

The changes in the mean velocity are also reflected in the velocity-fluctuation profiles. Figure 3 shows the non-dimensional intensity of the azimuthal velocity fluctuation ( $v_{rms} = v_{rms}^*/(r^*\Omega^*)$ ) plotted on a logarithmic scale against the wall-normal position. At  $R = 430$  and  $450$ , a maximum in  $v_{rms}$  is observed close to the disk due to the imbalance of the disk. This effect appears up to  $z \approx 2$ . At  $R = 510$ , the  $v_{rms}$  profile has developed a well-defined flow-induced maximum close to the wall. At higher Reynolds numbers, the velocity-fluctuation profiles reflect the development of a turbulent boundary-layer.

Figure 4 shows the development of the disturbance spectrum measured at  $z = 1.3$  for various  $R$ . The power spectral amplitudes  $P(\omega^*)$  are calculated from the ensemble-averaged time series and are plotted against the non-dimensional quantity  $\omega^*/\Omega^*$ . Linear stability theory shows that the flow is

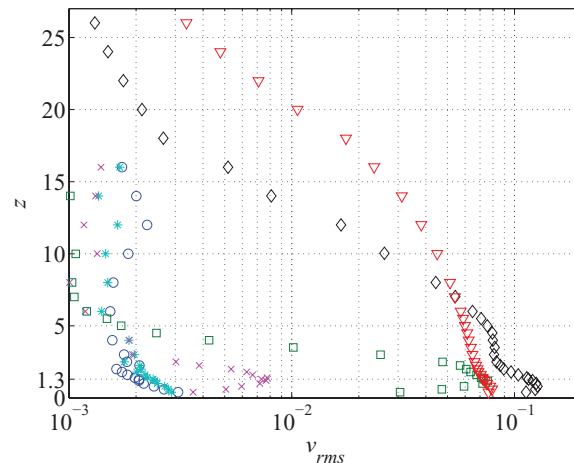


FIG. 3. Profiles of  $v_{rms}$ . The symbols are the same as in Fig 2.

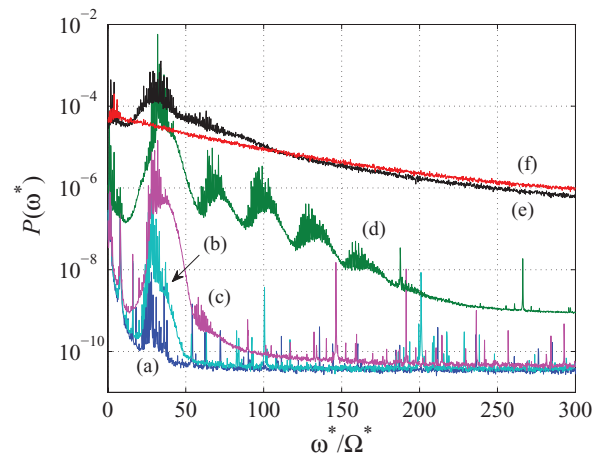


FIG. 4. Fourier power spectra for ensemble-averaged time series measured at  $z = 1.3$  at (a)  $R = 430$ , (b)  $R = 470$ , (c)  $R = 510$ , (d)  $R = 550$ , (e)  $R = 590$ , and (f)  $R = 630$ .

convectively unstable to stationary disturbances above about  $R = 290$ .<sup>5</sup> At  $R = 430$  one can observe a broad peak centered around  $\omega^*/\Omega^* = 30$  in Fig. 4. The amplitude of this peak increases with Reynolds number and corresponds to previous experimental studies that show between 28 and 32 stationary vortices.<sup>1</sup> Note that these stationary vortices are the result of the continuous excitation by unavoidable roughnesses fixed to the disk; it is known, however, from Lingwood<sup>5</sup> that the azimuthal wavenumber at the onset of absolute instability of the rotating-disk flow (corresponding to a traveling disturbance) is 68. For  $R = 510$ , a harmonic of the basic frequency appears and at  $R = 550$  at least five harmonics can be observed. The onset of nonlinearity is in accordance with the suggestion of Lingwood<sup>5,6</sup> that there is an absolute instability above  $R = 507$  and its role is to trigger nonlinearity and the onset of transition despite the fact that the disturbance amplitude at  $R \approx 510$  is quite small, less than 0.8% of the disk velocity. At  $R = 590$ , only the remnant of the primary peak remains with the remainder of the spectrum filled out; by  $R = 630$ , the spectrum reflects the turbulent nature of the boundary-layer.

In Fig. 5, the growth of the disturbances is shown from measurements of  $v_{rms}$  as a function of Reynolds number, where the Reynolds number was increased by moving the probe in the radial position (case I01 in Table I). The measurements were made at a constant height  $z = 1.3$  because,

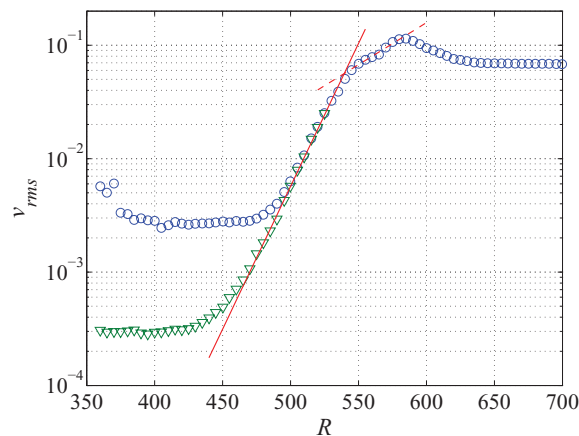


FIG. 5.  $v_{rms}$  variance measured at  $z = 1.3$  and a constant rotational speed  $\Omega^* = 1400$  rpm. Solid and dashed lines are exponential fittings for each instability region given as  $v_{rms} \sim \exp(\alpha R)$ , where  $\alpha$  is the growth rate. These coefficients for solid and dashed lines are  $\alpha = 0.058$  and  $0.017$ , respectively. Circles denote unfiltered signal, triangles show band-pass filtered signal ( $17 < \omega^*/\Omega^* < 70$ ) below  $R \leq 490$  and high-passed filtered signal ( $17 < \omega^*/\Omega^*$ ) for  $495 \leq R \leq 525$ .

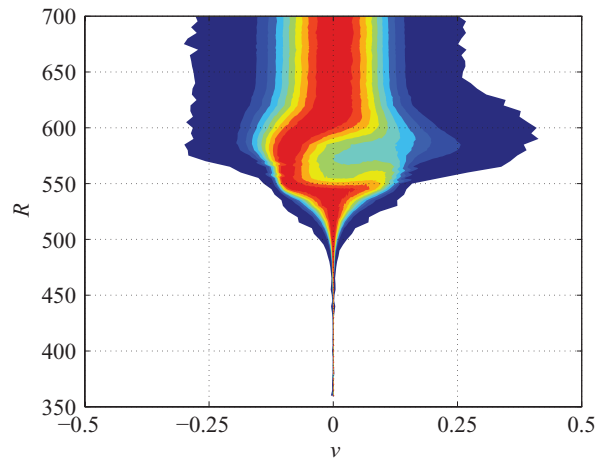


FIG. 6. The PDF of the filtered instantaneous azimuthal fluctuation velocity  $v$  at  $z = 1.3$  normalized by the wall speed. Filled contours indicate 10%, 20%, 30%, 40%, 50%, 60%, 70%, 80%, and 90% of the local PDF value.

in the unstable region, the intensity of  $v_{rms}$  has a maximum around that position as suggested in Fig. 3. The data shown are both the directly measured signal, as well as filtered signals. At low  $R$  the noise level is high compared to the amplitude of the fluctuations, mainly due to the imbalance of the disk and vibration of the traverse, but through band-pass filtering around the basic frequency the noise level can be lowered by an order of magnitude. For  $R \geq 495$ , the signal is instead high-pass filtered in order not to exclude the harmonics that start to appear above this  $R$ . For the filtered signal an exponential growth,  $v_{rms,filtered} \sim \exp(\alpha R)$ , is observed in the region  $475 < R < 530$ , with  $\alpha = 0.058$ . This is in agreement with the maximum growth rate for stationary linear disturbances in this  $R$  range (see, e.g., Figure 6a in Ref. 10, note that for spatially growing disturbances  $\alpha$  varies with  $R$ ). Also beyond  $R = 530$ , there is exponential growth but with a smaller ( $\sim 0.017$ ) rate. Around  $R = 580$ ,  $v_{rms}$  reaches a maximum value and thereafter it decreases to a constant level.

It is worth comparing Fig. 5 with Figure 4 of Viaud *et al.*<sup>11</sup> where the transition to turbulence of the disk boundary-layer flow in an open rotating cavity is described as a secondary instability of the global mode confirming via DNS the possibility of a direct transition mechanism for a real flow through a steep global-mode cascade. By comparison, the change in slope at around  $R = 545$  in Fig. 5 could correspond to Viaud *et al.*'s so-called "secondary front" where the secondary instability of the primary global mode sets in a little way downstream of the primary global mode, leading to a cascade of absolutely unstable secondary instabilities and transition to turbulence. If so, then the present results may represent the first experimental validation of Viaud *et al.*'s DNS results and Pier's<sup>7</sup> theoretical predictions of absolute instability of the primary global instability.

The growth rate curve shown in Fig. 5 does not show any details of how the flow structures change during the transition process. We propose here a new way to present the flow data that makes it possible to gain a better insight into the different stages of the transition process. By plotting the PDF of the fluctuating signal, where the velocity is normalized with the wall velocity and the PDF amplitude with its maximum value, an interesting picture is obtained. Figure 6 shows the resulting color contour plot of the PDF for the same data as in Fig. 5. Even a cursory glance of Fig. 6 gives a vivid impression of the changes in characteristics with Reynolds number and particularly at  $R = 550$ .

The PDF is narrow and almost constant up to  $R = 475$  due to the background noise and low fluctuation level. At about  $R = 475$ , the plot is seen to spread exponentially, as also suggested by Fig. 5. But at  $R = 550$ , the structure of the PDF has changed dramatically and is strongly skewed. This Reynolds number corresponds to the point where the slope of the exponential growth of  $v_{rms}$  changes in Fig. 5. Figure 6, however, supplies more information compared with Fig. 5 with regard to the structure of the disturbances. At around  $R = 600$ , the skewed PDF starts to disappear and the positive deviation of  $v$  has its maximum. The almost symmetric PDF above  $R = 650$  indicates that

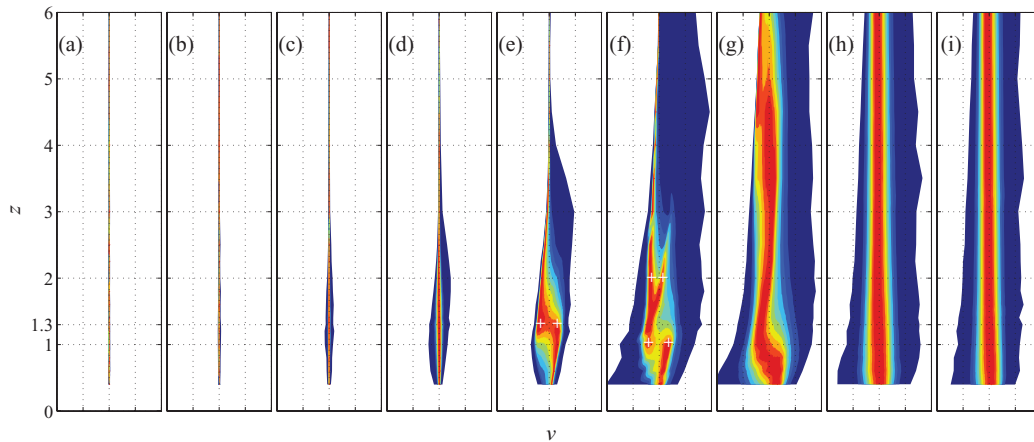


FIG. 7. The PDF of the instantaneous azimuthal fluctuation velocity normalized by the wall speed to show the  $z$ -structure at (a)  $R = 470$ , (b)  $R = 490$ , (c)  $R = 510$ , (d)  $R = 530$ , (e)  $R = 550$ , (f)  $R = 570$ , (g)  $R = 590$ , (h)  $R = 610$ , and (i)  $R = 630$ , namely cases P02 to P09 in Table I. Filled contours indicate same as Fig. 6. The range of the abscissa is  $-0.5$  to  $+0.5$  for all  $R$ . Note that in the free stream far above the disk, the positive values of  $v$  emanates from the high velocity fluid near the disk giving a positive skewness, i.e., the picture here is opposite to the one that would be observed for the flow over a stationary plate where the skewness is negative close to the boundary-layer edge. The white + signs in (e) and (f) show the position of the double peaks.

the flow has reached a fully developed turbulent state. These characteristics are not obvious in the spectral distributions such as those in Fig. 4.

This PDF method is also useful to capture the structure normal to the wall associated with the instability. Figure 7 shows the same quantity as plotted in Fig. 6, but at fixed Reynolds numbers (increasing by 20 units in each subplot) giving the PDF structure normal to the wall. Below a Reynolds number of 530, the PDF is symmetric around the mean value across the boundary-layer, indicating that the disturbance is near linear below this Reynolds number. By  $R = 550$  the PDF becomes strongly asymmetric and around in  $z = 1.3$  (Fig. 7(e)) a double peak has appeared marked with + in the figure. At  $R = 570$ , the picture is complicated further by the appearance of two double peaks, one around  $z = 1$  and the other around  $z = 2$ . For even higher Reynolds numbers, the maximum of the PDF again becomes centered around the mean value, which here is indicative of the flow becoming fully turbulent.<sup>12</sup>

In Fig. 7, an interesting phenomenon is captured at  $R = 570$ . Kohama<sup>2</sup> suggested that the secondary instability of the stationary primary vortices (observed using smoke-flow visualization) takes the form of “ring-like vortices which occur on the surfaces of each spiral vortices [sic]”. The two peaks in Fig. 7(f) of the PDF around  $z = 2.0$ – $2.8$  may be a manifestation of the secondary instability observed by Kohama. From a theoretical analysis, Balachandar<sup>13</sup> suggested that secondary vortices are centered over the saddle point of the primary cross-flow vortices. At the same  $R$  the position of the primary vortices change from  $z = 1.3$  to  $z = 1.0$ , which explains why the strong skewed PDF is observed in Fig. 6 above  $R = 550$ . Figures 6 and 7 together illustrate the structure of the boundary-layer flow through the transition process, comparing well with Viaud *et al.*'s<sup>11</sup> Figure 3 showing the nonlinear evolution of an initial perturbation to a disordered state. While not conclusive at this stage, the results shown here support previous experimental,<sup>2</sup> theoretical,<sup>7,13</sup> and numerical<sup>11</sup> suggestions of a global nonlinear mode that is itself unstable to secondary perturbations.

As discussed in Ref. 14, the maximum convective linear growth rate above  $R = 507$  is much larger than the absolute growth rate but given sufficient time the amplitude of disturbances generated by the absolute instability will become large enough to cause nonlinearities and to fix the radial position of the onset of the transition process. As Huerre and Monkewitz<sup>15</sup> suggested the nonlinear global mode resulting from a finite region of local absolute instability may be thought of as a highly repeatable “self-excited, low-amplitude wavemaker....,” which acts as a source for the downstream instability wave(s). Furthermore, as discussed by Viaud *et al.*,<sup>11</sup> in a strongly nonlinear and weakly non-parallel

regime, the presence of a finite region of absolute instability has been shown theoretically to be a sufficient condition for a nonlinear global mode with a steep front (a so-called “elephant mode”), located at the upstream boundary (primary front) between local convective and absolute instability, and, further, when the global mode is itself absolutely unstable to local secondary perturbations the transition process is likely to be via the secondary instabilities a short distance downstream of the primary front.<sup>2,7,11</sup>

To summarize, the present work shows a new way to describe the characteristics of a rotating-disk flow by introducing the PDF contour plot of the normalized fluctuation velocity (where the PDF at each  $z$ -position is normalized by its maximum value). The map is shown in Fig. 6 and if compared with spectral and rms distributions in Figs. 4 and 5 it shows the different stages more clearly. It is shown that the PDF can identify an exponentially growing instability, a secondary instability and also clearly shows the onset of the fully developed turbulent flow. In addition, this method is applied to the velocity profile measurements to capture the structure normal to the wall. PDF contour plots at each Reynolds number clearly show the disturbance structure, in particular, peaks in the PDF at  $R = 570$  may be associated with a secondary instability. Moreover, the evidence presented herein may represent the first experimental validation of the suggested secondary absolute instability of the primary nonlinear (steep-fronted) global mode.<sup>7,11</sup> As mentioned above, this PDF method may be useful not only for rotating-disk flows (the so called BEK system of rotating boundary-layer flows<sup>9</sup>), but also for other transitional flows, for example other three-dimensional boundary-layers, such as those over swept wings, or even more conventional two-dimensional boundary-layer configurations.

This research is supported by the Swedish Research Council (VR) and KTH. We also acknowledge the help from late Dr. Tim Nickels in arranging the loan of the experimental apparatus from the University of Cambridge Department of Engineering to KTH. We also thank the referees for useful comments and for pointing out Ref. 11 to us.

- <sup>1</sup> N. Gregory, J. T. Stuart, and W. S. Walker, “On the stability of three-dimensional boundary layers with application to the flow due to a rotating disk,” *Philos. Trans. R. Soc. London* **248**, 155 (1955).
- <sup>2</sup> Y. Kohama, “Study on boundary layer transition of a rotating disk,” *Acta Mech.* **50**, 193 (1984).
- <sup>3</sup> R. J. Lingwood, “An experimental study of absolute instability of the rotating-disk boundary-layer flow,” *J. Fluid Mech.* **314**, 373 (1996).
- <sup>4</sup> T. C. Corke, E. H. Matlis, and H. Othman, “Transition to turbulence in rotating-disk boundary layers – convective and absolute instabilities,” *J. Eng. Math.* **57**, 253 (2007).
- <sup>5</sup> R. J. Lingwood, “Absolute instability of the boundary layer on a rotating disk,” *J. Fluid Mech.* **299**, 17 (1995).
- <sup>6</sup> R. J. Lingwood, “Absolute instability of the Ekman layer and related rotating flows,” *J. Fluid Mech.* **331**, 405 (1997).
- <sup>7</sup> B. Pier, “Finite-amplitude crossflow vortices, secondary instability and transition in the rotating-disk boundary layer,” *J. Fluid Mech.* **487**, 315 (2003).
- <sup>8</sup> A. V. Johansson and P. H. Alfredsson, “On the structure of turbulent channel flow,” *J. Fluid Mech.* **122**, 295 (1982).
- <sup>9</sup> R. J. Lingwood and S. J. Garrett, “The effects of surface mass flux on the instability of the BEK system of rotating boundary-layer flows,” *Eur. J. Mech. B/Fluids* **30**, 299 (2011).
- <sup>10</sup> Z. Hussain, S. J. Garrett, and S. O. Stephen, “The instability of the boundary layer over a disk rotating in an enforced axial flow,” *Phys. Fluids* **23**, 114108 (2011).
- <sup>11</sup> B. Viaud, E. Serre, and J.-M. Chomaz, “Transition to turbulence through steep global-modes cascade in an open rotating cavity,” *J. Fluid Mech.* **688**, 493 (2011).
- <sup>12</sup> P. H. Alfredsson, R. Örlü, and P. Schlatter, “The viscous sublayer revisited – exploiting the self-similarity to determine the wall position and friction velocity,” *Exp. Fluids* **51**, 271 (2011).
- <sup>13</sup> S. Balachandar, C. L. Streett, and M. R. Malik, “Secondary instability in rotating-disk flow,” *J. Fluid Mech.* **242**, 323 (2006).
- <sup>14</sup> R. J. Lingwood, “On the application of the Briggs’ and steepest-descent methods to a boundary-layer flow,” *Stud. Appl. Math.* **98**, 213 (1997).
- <sup>15</sup> P. Huerre and P. A. Monkewitz, “Local and global instabilities in spatially developing flows,” *Annu. Rev. Fluid Mech.* **22**, 473 (1990).